A biomechanical model for cell sensing and migration

Arnaud Chauvière, Ian Manifacier, Claude Verdier, Grégory Chagnon, Ibrahim Cheddadi, Nicolas Glade, Angélique Stéphanou

A biomechanical model for cell sensing and migration

Arnaud Chauvière[1], Ian Manifacier[1], Claude Verdier[2], Grégory Chagnon[1], Ibrahim Cheddadi[1], Nicolas Glade[1], and Angélique Stéphanou[*1]

[1]*Univ. Grenoble Alpes, CNRS, UMR 5525, VetAgro Sup, Grenoble INP, TIMC, 38000 Grenoble, France*

[2]*Univ. Grenoble Alpes, CNRS, LIPhy, 38000 Grenoble, France*

Abstract

We developed an original computational model for cell deformation and migration capable of accounting for the cell sensitivity to the environment and its appropriate adaptation. This cell model is ultimately intended to be used to address tissue morphogenesis. Hence it has been designed to comply with four requirements: (1) the cell should be able to probe and sense its environment and respond accordingly; (2) the model should be easy to parametrize to adapt to different cell types; (3) the model should be able to extend to 3D cases; (4) simulations should be fast enough to integrate many interacting cells. The simulations carried out focused on two aspects: first, the general behaviour of the cell on a homogeneous substrate, as observed experimentally, for model validation. This enabled us to decipher the mechanisms by which the cell can migrate, highlighting respective influences of the adhesions lifetimes and their sensitivity to traction; second, it predicts the sensitivity of the cell to an anisotropic patterned substrate, in agreement with recently published experiments. The results show that mechanosensors simulated by the model make it possible to reproduce such experiments in terms of migration bias generated by the substrate anisotropy. Here again, the model provides a biomechanical explanation of this phenomenon, depending on cell-matrix interactions and adhesion maturation rate.

Keywords: cell morphology, focal adhesion, mechanosensor, patterned substrate, stress fibres.

[*]angelique.stephanou@univ-grenoble-alpes.fr

1 Introduction

Cell motility, *i.e.* cell deformation and migration has been studied for many decades both on two–dimensional substrates (Abercrombie et al. 1970, Abercrombie 1980, Theriot & Mitchison 1991) or in 3D (Yamada et al. 2022). Indeed the cell ability to migrate in complex media underpins a number of fundamental biological processes including embryogenesis, wound healing, angiogenesis, cell invasion and metastasis (Peschetola et al. 2013, Kulesa et al. 2021, Bouchalova & Bouchal 2022). But the mechanisms of motility are difficult to understand because they involve the complex interplay between actin dynamics at the cell edge (Theriot & Mitchison 1991), contractility through acto-myosin dedicated assembly/disassembly (Chi et al. 2014), retrograde flow (Kruse et al. 2006), as well as coordinated links between the cytoskeleton and focal adhesions (Galbraith et al. 2007). Finally, the modes of migration used by cells (i.e. mesenchymal or ameboid) can be strongly influenced by confinement (Liu et al. 2015), in particular in 3D rich–filamentous networks (Starke et al. 2013).

To decipher the various mechanisms at play, many theoretical models, either mathematical or computational, have been developed at the scale of the single cell. The cystokeletal actin dynamics in relation with the formation of adhesions is at the heart of many studies (Gardel et al. 2008, Chandra et al. 2022), although some models focus more on the membrane, hydrostatic pressure and intracellular contractility-generated fluxes (Petrie et al. 2014, Woolley et al. 2017). Other theoretical models have allowed to clarify the roles, regulatory activities and relationships of key proteins such as Cdc42, Rac (Marée et al. 2006), rho GTPases (Holmes et al. 2016, Rens & Edelstein-Keshet 2019) and Arp2/3 (Garner & Theriot 2022). They have also helped identify the physical mechanisms required for cell elongation, translocation and motion as a combination of focal adhesions formation and stress fibre maturation and turnover (Franco et al. 2010, Vernerey & Farsad 2014).

More recently, the necessity to integrate cell interactions with its environment in the models has been highlighted (Eichinger et al. 2021). Chemoattraction used to be considered as a major driver of cell migration, but the focus is now more specifically on the cell-matrix biomechanical interactions. A plethora of models have stressed the importance of these bidirectional interactions (Muntz et al. 2022, Yamada et al. 2022, Akbarzadeh Solbu et al. 2023). On the one hand cell sensing allows to detect the properties of the matrix in terms of surface ligands and bulk mechanical properties leading to the formation of adhesions and the build up of traction forces (Gardel et al. 2008). On the other hand the matrix can be remodeled, *i.e.* deformed (Schluter et al. 2012, Reinhardt et al. 2013), degraded (Zhu & Mogilner 2016, Heck et al. 2020) or synthesized by the cell. Those dynamically changing properties reciprocally affect the interaction with the cell (Stéphanou et al. 2015). That is why understanding this dynamical relationship is considered a major therapeutic challenge (Yamada et al. 2022).

A thorough review of the literature shows that there are many existing models, but none of them answer all the questions emphasized above. Models by Zhu & Mogilner (2016) and Satulovsky et al. (2008) allow to gener-

ate a great diversity of cell shapes and behaviours, but they are computationally costly. Models that address the cell cytoskeleton with nodes and springs are usually more efficient and well adapted for sensing the environment stiffness (Kim et al. 2013, Bangasser et al. 2017), but lack the probing ability. Kim et al. developed a model for filopodia sensing in 3D but at the cost of an increased complexity (Kim et al. 2015, 2018). The agent-based model by Heck et al. (2020) and the cellular Potts model by Rens & Merks (2020) are well adapted to probe and sense the extracellular matrix, however they cannot be easily generalized to address cell migration in a 3D environment.

We note that the paper by Merino-Casallo et al. (2022) could fit most of our requirements. The model describes mesenchymal migration as a 3-step process including probing, pathways activation and cell translocation. The probing phase is based on chemosensing that activates a signaling network involving cytosolic PI3K regulating protrusion dynamics. One of the highlight of this model is to take into account the steric constraints, that is the ability of the cell to squeeze through the extracellular matrix (ECM) pores. For that the plasma membrane is represented to delineate the space occupied by the cell. This allows to calculate a friction term which is used to represent the steric hindrance, *i.e.* the difficulty encountered by the cell to migrate through the dense 3D ECM. Although appealing, this model takes into account the plasma membrane and molecular dynamics that we wished to avoid to reduce the computational cost.

In this paper our goal was to develop an efficient model for cell sensing with in mind the future idea to address many cell-cell interactions (up to a hundred cells) in a 3D matrix. This will allow to investigate cell-matrix remodelling in connection with cell auto-organization and applications to wound healing, angiogenesis or cell invasion. To achieve this objective, we had to comply to the following requirements: (1) cell ability to probe and sense the environment and respond accordingly; (2) efficient parametrization to adapt to different cell types; (3) easy extension to 3D cases; (4) fast simulations to integrate many interacting cells.

The model proposed is directly inspired from a previous one describing the synchronized maturation of actin stress fibres and focal adhesions (Stéphanou et al. 2008, Stéphanou 2009, Franco et al. 2010). The hybrid model was coupling PDEs for the actin dynamics and force generation with an algorithm describing the formation of discrete independent adhesion sites and their maturation. However the model was strictly limited to 2D and simulations were slow. We reconsidered this initial model, assuming that the cytoskeletal fibres and adhesion proteins were not a limiting factor (always available in sufficient amount). As a consequence, the cell membrane that delineates the intracellular space was not required. The actin cytoskeletal fibres could radiate from the cell centre and form adhesions at their ends. We retained from the original model the reciprocal maturation of the cytoskeletal fibres and their associated adhesions as the fundamental key for cell sensing. Three levels of maturation were considered. The first one corresponds to an exploratory phase with dynamic adhesions progressively maturating by increasing the adhesion strength while reducing their dynamic turnover (2nd phase). In the last phase the adhesion is anchored

and the fibre can reciprocally develop higher forces required for cell translocation hence migration.

The model strength relies on the dynamic adaptation of the motile cell to the environment. Its ability to detect an adhesive environment was first tested in 2D on a homogeneous substrate, then on an anisotropic one. The simulations reproduced the well-known experimental behaviours regarding the relationship between velocity and adhesion strength (Palecek et al. 1997, Caballero et al. 2014). Then migration biases were introduced through an anisotropic environment – as observed in a recent experimental setup (Lo Vecchio et al. 2020) – and could also be reproduced and explained on a qualitative basis. The model appears to be a reliable simulation tool to further tackle more complex cell-matrix interactions involving matrix remodelling.

2 Cell model

2.1 Biological motivation and main assumptions

Our aim was to develop a relatively simple cellular model to subsequently address cell auto-organization and different processes of morphogenesis. Although simple, the model should capture the main mechanisms responsible for cell migration. Moreover, in order to attain its future goal, the model developed had to comply to a number of constraints. Those constraints are:

1. the cell should be able to probe and sense its environment and to respond adequately to it;
2. the model should be easy to parameterize to adapt to different cell types context (since we envisaged to model different processes of morphogenesis);
3. the model should be easy to extend to 3D;
4. the simulation should not be costly in term of calculation time, since we intend to subsequently integrate numerous interacting cells (from several hundred to thousands of cells).

There is a consensus on how mesenchymal migration proceed: the cell exhibits membrane protrusions sustained by actin fibres; makes adhesions to the extracellular matrix through integrins; actomyosin fibres contract to allow the cell to move forward by taking support on the adhesions, that ultimately break. Many different protein are involved and adhesions and cytoskeleton turnover is well orchestrated to allow the cell to renew the all process to migrate (Mavrakis & Juanes 2023). As in most biomechanical models, we made the choice not to describe the complex protein regulations. On the other hand, we integrated coupled adhesions and fibres reinforcement through three maturation stages to reproduce the protrusion-adhesion-translocation sequence in a dynamical way.

Although the shape that a cell can take can be complex, it is common to represent it with radial fibres. Those fibres are given (visco)elastic properties and generate forces on the nucleus at one end, and an adhesion at the other end (Bangasser et al. 2017, Isomursu et al. 2022, Kim et al. 2013). The force competition between the fibres will ultimately condition the cell displacement. We chose to consider radiating elastic fibres that stand for actin cables that later mature, with the recruitment of myosin, into stress fibres. The sensing property of the cell is due to filopods, that are short actin fibre extensions. We integrate this structure into the model which develops where adhesions form.

Currently there is no extracellular matrix in the model. The environment is considered as a substrate – whose nature is not specified – on which the cell can form adhesions. The modulation of the adhesion strength is used as a proxy to simulate different matrices characteristics (it can account for different concentrations of ligands and/or a differential cell-matrix affinity).

2.2 Overall cell structure

The cell model is constructed to account for the overall cell dynamics based on the interactions between cytoskeletal fibres and focal adhesions. It is composed of branches and nodes that form a hierarchical tree like structure meant to represent the mechanical structure of the cell by emulating its centre (nucleus), membrane protrusions, adhesions and mechanosensors. Each node N_i has an order i (from 0 to 2) that indicates its degree of separation from the central node N_0. The parent node of N_i is node N_{i-1} for $i > 0$. Several N_i nodes can radiate from a node N_{i-1} and each branch B_i connects the two nodes N_{i-1} and N_i.

- The N_0 node represents the cell centre, (*i.e.* the cell nucleus). This point is unique and it is used to locate the cell.
- The N_1 node represents a cell adhesion as the tip of a B_1 branch , *i.e.* a protrusion emanating from the cell centre. N_1 nodes have the potential to maturate and exist under three different forms of increased maturity (described below) in order to account for the evolving nature of the cell adhesions.
- The N_2 node represents a mechanosensor at the extremity of a B_2 branch. Those typically represent membrane extensions, such as filopodia, probing the cell environment.

The number, position and properties of nodes and branches are dynamically regulated, such that the cell generates or deletes nodes and branches. The latter transmit and generate forces thus enabling nodes to move and pull on the substrate. The cell can consequently spread, adhere, pull and move. The behaviour of each node is dependent on its order, thus enabling the emergence of a coherent system. The rules regulating each node type are summarized

in Figure 1 and are detailed below.

2.3 Nodes generation

N_1 nodes

N_1 is the main adhesion that undertakes a maturation process eventually leading to a focal adhesion able to sustain cell translocation (higher force) so that the cell migrates. Several N_1 nodes can be generated during the cell's life time. The frequency and the location at which they are generated are regulated in a probabilistic manner. Therefore, to determine how many N_1 nodes should be generated during the current time step, we first need to calculate the occurrence of independent events that will attempt to generate them. To do so, we define the mean frequency ν_1 at which these independent events occur around the cell. But, to avoid overcrowding of N_1 nodes in one area, an exclusion angle $\delta\theta_1$ is defined around the B_1 branch, so as to prevent new N_1 nodes from forming too close to their already existing neighbours (Fig. 2). From there we can then calculate λ_1, the expected rate of occurrence during a time step dt:

$$\lambda_1 = \nu_1 dt \tag{1}$$

Then we use a pseudo-random variate generator that follows the Poisson's distribution with λ_1 as input. The obtained random variate integer j_1 is the number of events that will attempt to create a N_1 node during the current time step. If j_1 is greater than zero and if there is room to create a new node, then a new node is created at a fixed initial distance l_{10} from N_0 at a randomly generated angle θ_1 (Fig. 2). This angle is a random variate pulled from a uniform distribution over the angular domain that remains available. This process is repeated j_1 times or until there is no more room to create another node because the angular domain is fully inhibited.

N_2 nodes

N_2 nodes can be considered as membrane spikes probing the cell environment. N_2 nodes are stochastically emitted by the parent N_1 node with a mean frequency ν_2 depending on the maturation level of N_1. An immature N_1 emits N_2 nodes with a higher frequency to actively probe the environment and orient the cell displacement. As it maturates, the N_1 node reinforces its adhesion strength to the substrate and emits N_2 nodes with a lower frequency to progressively reduce the probing activity and stabilize the adhesion. The expected rate of occurrence λ_2 of a new N_2, during a time step dt, is:

$$\lambda_2 = \nu_2 dt \tag{2}$$

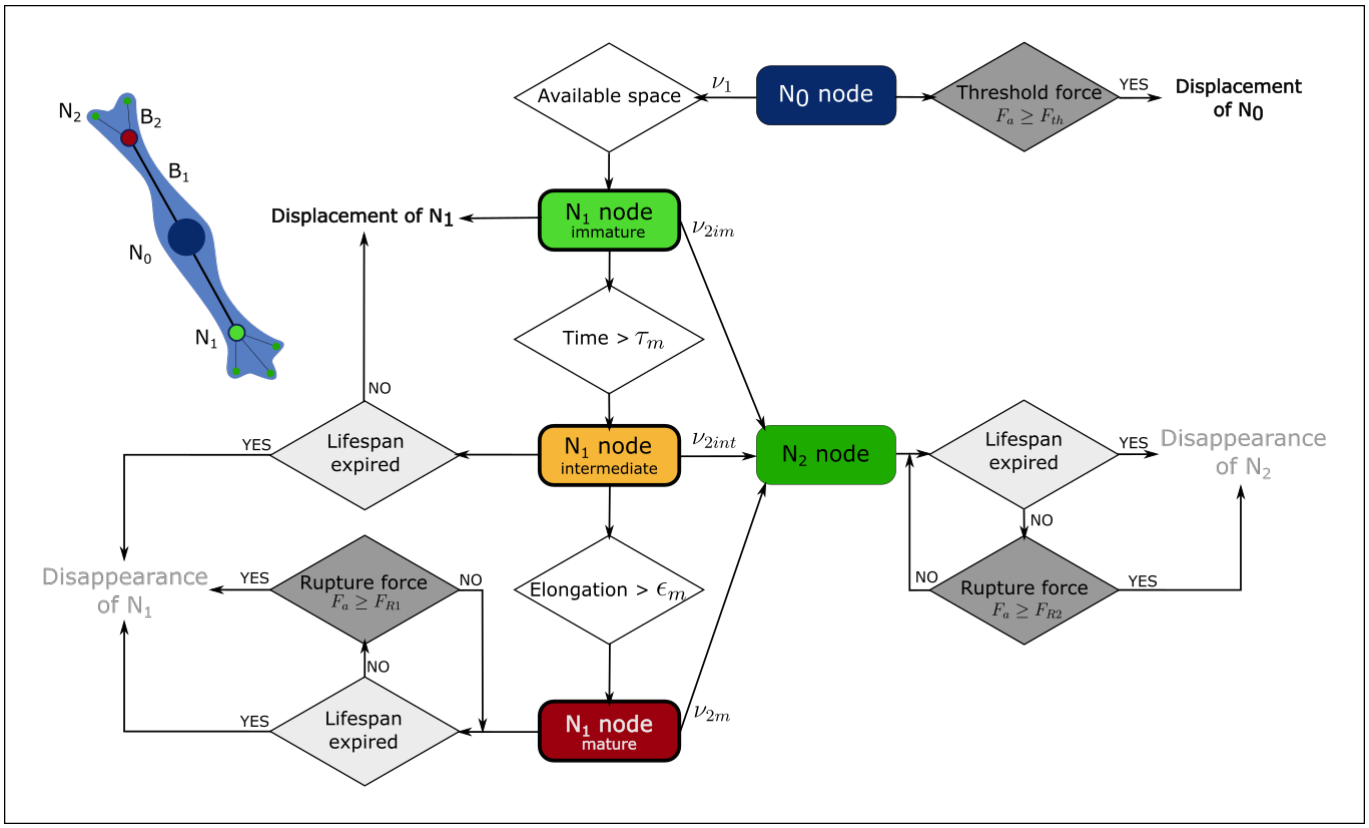

Figure 1: The cell structure is composed of nodes and branches, N_0, the root node is at the centre, B_1 branches connect the root node to N_1 nodes and B_2 branches connect the latter to N_2 nodes. The flowchart shows how nodes evolve in time. The N_0 node is bound to the substrate and moves if the adhesion force F_a is greater than the threshold force F_{th}. It generates N_1 nodes if space is available. N_1 nodes are initially immature, then intermediate and finally mature. The respective function of each N_1 state is to: explore (if immature), assess if it can become mature (if intermediate) and bind to the substrate (if mature). During each maturation state a N_1 node respectively generates N_2 nodes at an average stochastic rate of ν_{2im}, ν_{2int} and ν_{2m}. The function of the N_2 nodes is to probe the environment and contribute to the movement of the cell's leading edge. Therefore, immature and intermediate N_1 nodes move, while mature N_1 nodes are bound to the substrate. Immature N_1 nodes transit to an intermediate state after reaching the age τ_t, while the mature state is reached once the B_1 branch is strained above ε_m. When the adhesion force F_a of a N_1 or N_2 node is greater than the respective rupture force F_{R1} or F_{R2}, there is rupture and the node disappears and its child nodes with it.

A Poisson's variate generator is used to define the number of N_2 nodes that are created during the time step with λ_2 as input. Then the angle with which each new N_2 appears, is defined using a uniform-random variate generator that follows a uniform distribution. The sample space is defined between $\theta_1 \pm \delta\theta_2$. The new N_2 node is thus created at the angle θ_2 and fixed at an initial distance l_{20} from the position of the parent N_1 node (Fig. 2).

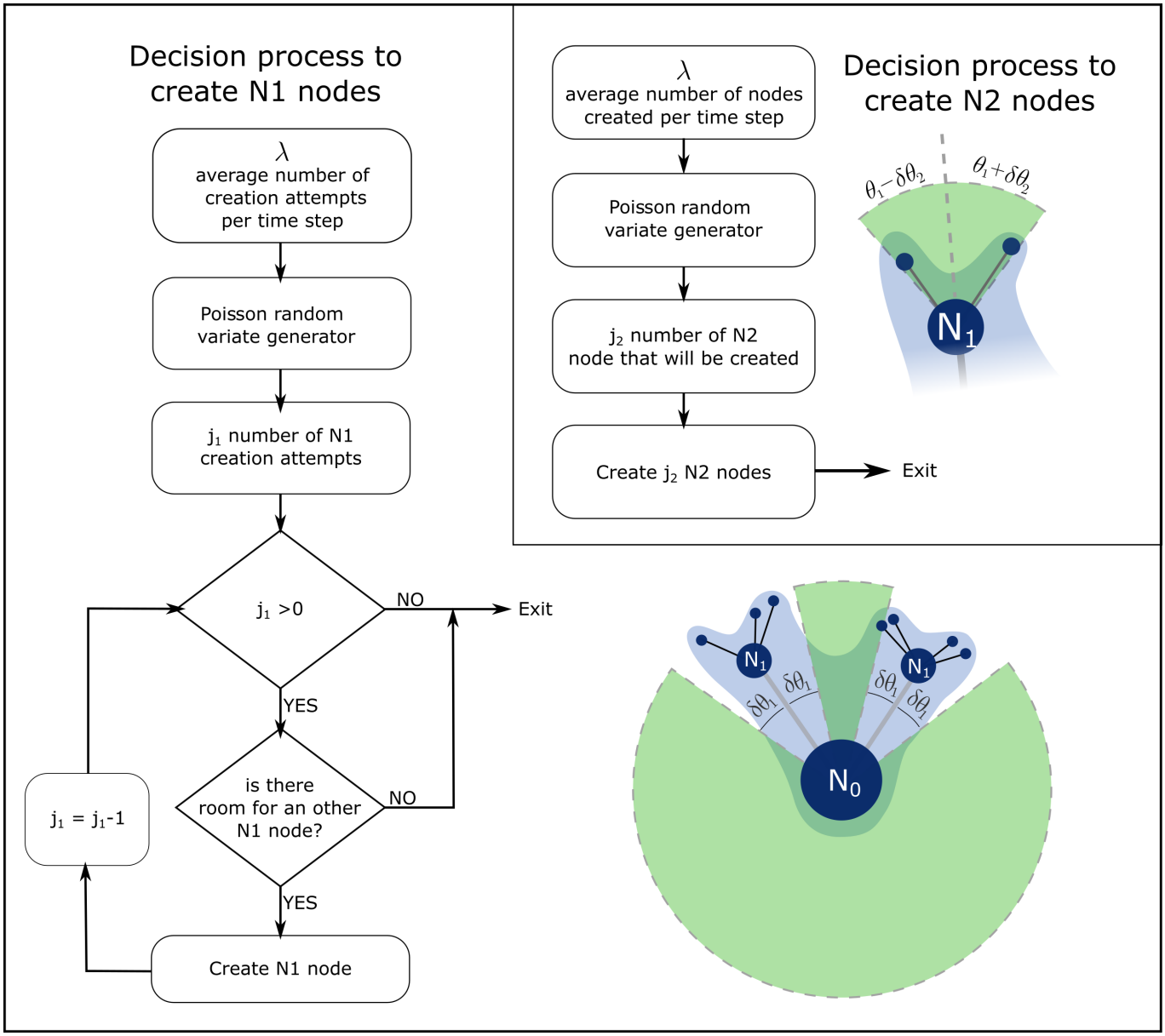

Figure 2: Nodes creation. *Left and bottom:* decision process to create N_1 nodes at each time step. A N_1 node located at an angle θ_1 will inhibit the formation of new N_1 nodes in the angular domain surrounding the B_1 branch *i.e.* $\theta_1 \pm \delta\theta_1$. *Top right:* Decision process to create N_2 nodes at each time step in an angular domain surrounding the B_1 branch *i.e.* $\theta_1 \pm \delta\theta_2$. Areas in green represents the zone where a new node can be created.

2.4 Nodes displacement

Our model aims at describing the cell movement and displacement dynamics. Therefore the nodes adhering to the substrate with various degrees, that depend on their type and maturation level, can be displaced by the mechanical forces applied on them through the branches.

Each branch (of index i) connected to a node exerts a force $\mathbf{F}_i$ on the node such that the net force applied by the n branches on the node is the sum of these forces. If the node is bound to the substrate the adhesion force $\mathbf{F}_a$ prevents the node from moving such that:

$$\mathbf{F}_a = -\sum_{i=1}^{n} \mathbf{F}_i \tag{3}$$

On the other hand, when the node is able to move, according to the quasi-static approximation the acceleration is negligible. Thus using Newton's second law, and by stating that the friction force $\mathbf{F}_v = -\alpha\mathbf{v}$ is always opposed to the node's displacement with velocity $\mathbf{v}$, we have:

$$\alpha\mathbf{v} = \sum_{i=1}^{n} \mathbf{F}_i \tag{4}$$

where α is the friction coefficient of the node with the substrate. It depends on the node type and maturation level. The node's new position at the next iteration noted $\mathbf{x}_N^{t+dt}$ is thus given by:

$$\mathbf{x}_N^{t+dt} = \mathbf{x}_N^t + \mathbf{v}dt \quad \text{with} \quad \mathbf{v} = \frac{1}{\alpha}\sum_{i=1}^{n} \mathbf{F}_i \tag{5}$$

In our model, N_2 nodes play the role of sensors interacting with the substrate to probe its mechanical and/or adhesive properties in order to orient the cell displacement. Several N_2 nodes are simultaneously linked by B_2 branches to their parent node N_1 on which they pull. B_2 branches are assumed to be short elastic actin spikes with elastic coefficient κ_2. They are emitted with an initial length l_{20}, chosen to correspond to the length of a filopod and they are characterized by a predefined strain ε_{20} such that the resting length l_{2r} of the spike is smaller than its initial length, *i.e.* :

$$\varepsilon_{20} = \frac{l_{20} - l_{2r}}{l_{2r}} > 0 \tag{6}$$

Parameters are chosen so that the spike is initially stretched and will attempt to return to its rest length. This will cause the branch to pull on both nodes, giving rise to a positive elastic force F_{el} along the $\overrightarrow{N_1N_2}$ axis since the N_2 node is fixed (bounded to the substrate) and the N_1 node is free to move (at least in its non mature states):

$$F_{el} = max(0, \kappa_2(l_2(t) - l_{2r})) \quad \text{with} \quad l_{2r} = \frac{l_{20}}{1+\varepsilon_{20}} \tag{7}$$

The resulting force on the parent node N_1 is calculated as the sum of the elastic contributions of each B_2 branches with equation (4). The N_1 node is then displaced to its new position according to the vector v given in equation (5).

Since we neither take into account actin polymerisation dynamics nor the cell membrane in our model, actin retrograde flow - which is driven by the resistance of the membrane to actin polymerization at the leading edge (Parsons et al. 2010) - is not represented. However, the actin fibers corresponding to the B_1 branches pull on the N_1 adhesions creating a backward movement towards the cell center. At the immature state, this backward movement is counterbalanced by the probing activities of the N_2 nodes that allow to oriente the cell B1 branch extension towards the most favorable locations where the N_1 adhesion will stabilize.

2.5 Nodes maturation

The N_1 nodes represent the adhesion points on which the cell actin fibres, represented by the B_1 branches, take support. Before the cell is able to move, the adhesion initially composed of integrins, should be reinforced by the recruitment of new integrins via binders. These binders are recruited for the nucleation and binding of actin fibres, including talin, paxillin, vinculin, FAK, VASP, Arp2/3 (Legerstee & Houtsmuller 2021). The fibres can then generate increasing forces on the N_1 adhesion that reaches maturation under the form of a focal adhesion through the recruitment of zyxin and tensin (Zaidel-Bar et al. 2003). Reciprocally the mature N_1 adhesions can resist higher tensions from the cytoskeletal fibres. This bi-directional maturation process between adhesion and cytoskeletal fibres is important to realistically describe the cell sensing ability and its evolving biomechanics. Indeed, depending on the mechanical nature of the substrate the maturation process will be more or less efficient depending on the level of forces reached by the cell fibres (B_1 branches).

We consider in the model three levels of maturation for the N_1 nodes and its associated B_1 branch: immature, intermediate and mature states. Each successive state is characterized by an enhanced adhesiveness to the substrate and by an enhanced potential of force generation (Fig. 3 and Fig. 4).

- *Immature state:* the N_1 node is free to move and is displaced by the forces exerted by the N_2 nodes emitted at a higher rate ν_{2im} in this first state. Consequently its friction with the substrate is initially small with coefficient α_{10} and we propose that it increases linearly with time - as integrins and actin-bound proteins are progressively recruited with a typical timeframe (Parsons et al. 2010) - to reach the value α_{int} at time τ_t which characterizes the friction of the intermediate state. The friction evolution between the immature and

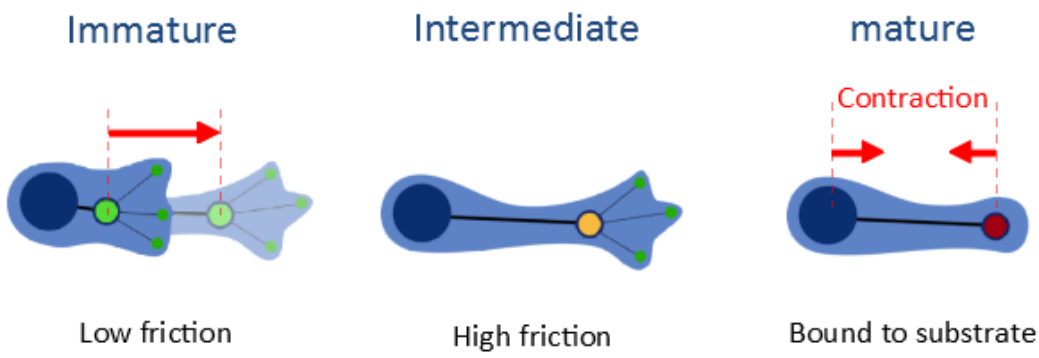

Figure 3: Illustration of the maturation stages of the $N1$ node. The immature node, characterized by a low friction with the substrate, is displaced by the traction of the N_2 nodes. After some pre-defined time the N_1 node reaches the intermediate maturation state characterized by an increased friction with the substrate. It finally reaches maturation if the B_1 branch is sufficiently elongated by the tensions from the N_2 nodes. The mature adhesion is bound to the substrate and the B_1 branch becomes contractile to generate higher forces on the N_0 node in order to allow the cell to translocate by taking support on the N_1 node to move forward.

intermediate states is thus given by:

$$\alpha_1(t) = \frac{\alpha_{int} - \alpha_{10}}{\tau_t} t + \alpha_{10} \tag{8}$$

As a concomitant event, the B_1 branch is progressively reinforced by actin fibres recruitment, that leads to a linearly increasing stiffness from κ_{10} (immature state) to κ_{11} (intermediate state):

$$\kappa_1(t) = \frac{\kappa_{11} - \kappa_{10}}{\tau_t} t + \kappa_{10} \tag{9}$$

The branch initially corresponds to an unstretched spring of length l_{10} that can bear tension and compression depending on the node displacement $l_1(t)$. The elastic restoring force in the branch is then given by:

$$F_{el} = \kappa_1(t)(l_1(t) - l_{10}) \tag{10}$$

- *Intermediate state:* it is reached when the N_1 node reaches the age τ_t for which the values of the friction coefficient and branch stiffness are kept constant as:

$$\alpha_1(t) = \alpha_{int} \quad \text{and} \quad \kappa_1(t) = \kappa_{11} \tag{11}$$

The increased friction coefficient of the node N_1 makes it more resistant to the displacement from the pulling N_2 nodes. Moreover, the production rate of N_2 nodes is concomitantly reduced with $\nu_{2int} < \nu_{2im}$. This reduces significantly the exploration potential of the branch. At this stage, the B_1 branch corresponds to a bundle of

actin fibres for which the rest length is reassessed and given by $l_1(\tau_t)$. The elastic restoring force in the branch is now given by:

$$F_{el} = \kappa_{11}(l_1(t) - l_1(\tau_t)) \tag{12}$$

- *Mature state:* it corresponds to the local culminating cell protrusion concomitant to the formation of a stable focal adhesion. The transition to this state only occurs if the B_1 branch elongation from its new resting length $l_1(\tau_t)$ reaches the elongation target ε_m, *i.e.* if:

$$\frac{l_1(t) - l_1(\tau_t)}{l_1(\tau_t)} \geq \varepsilon_m \tag{13}$$

This condition is not necessarily reached, so not all N_1 maturate to their final state. If they do, two major transitions affect the node and branch. First, the node is fixed, bound to the substrate, in order to be able to sustain cell translocation that is required for the cell displacement. The production rate of N_2 is further reduced with $\nu_{2m} < \nu_{2int}$. Second, the branch becomes contractile, through myosin recruitment, and corresponds to a stress fibre which is able to generate the force required for the cell translocation, *i.e.* the force that will allow the N_0 node to move. The contractile force F_c grows concomitantly with the increased resistance of the adhesion force F_a. We propose to represent it by mean of the following exponential function:

$$F_c = \gamma_{max}(1 - e^{-\frac{\|\mathbf{F}_a\|}{F_\gamma}}) \tag{14}$$

where γ_{max} is the stall force of the adhesion, F_γ is a characteristic force constant, and $\|\mathbf{F}_a\|$ is the norm of the adhesion force. The total force in the branch is the sum of the passive elastic contribution F_{el} (Eq. (12)) and active contractile one F_c (Eq. (14)). The cell translocation occurs if the adhesion force F_a (Eq. (3)) is big enough to support the tearing of the cell, corresponding to the threshold force F_{th}.

Regarding the N_1 branch maturation, we assume that the actin fiber is an elastic rod under tension at the initial stage. As the fibers maturate, fibers are recruited to form a bundle of fibers still possessing an elastic property. The contractile contribution on the other hand is an active process and involves the recruitment of myosin. The actomyosin fibers are responsible for the cell contractility. This process comes into play at the end of the maturation process of the actin fibers, which correspond to stress fibers at this stage of maturation. The active contractile force is much higher than the passive elastic force and dominates to generate the traction force required for cell translocation leading to migration.

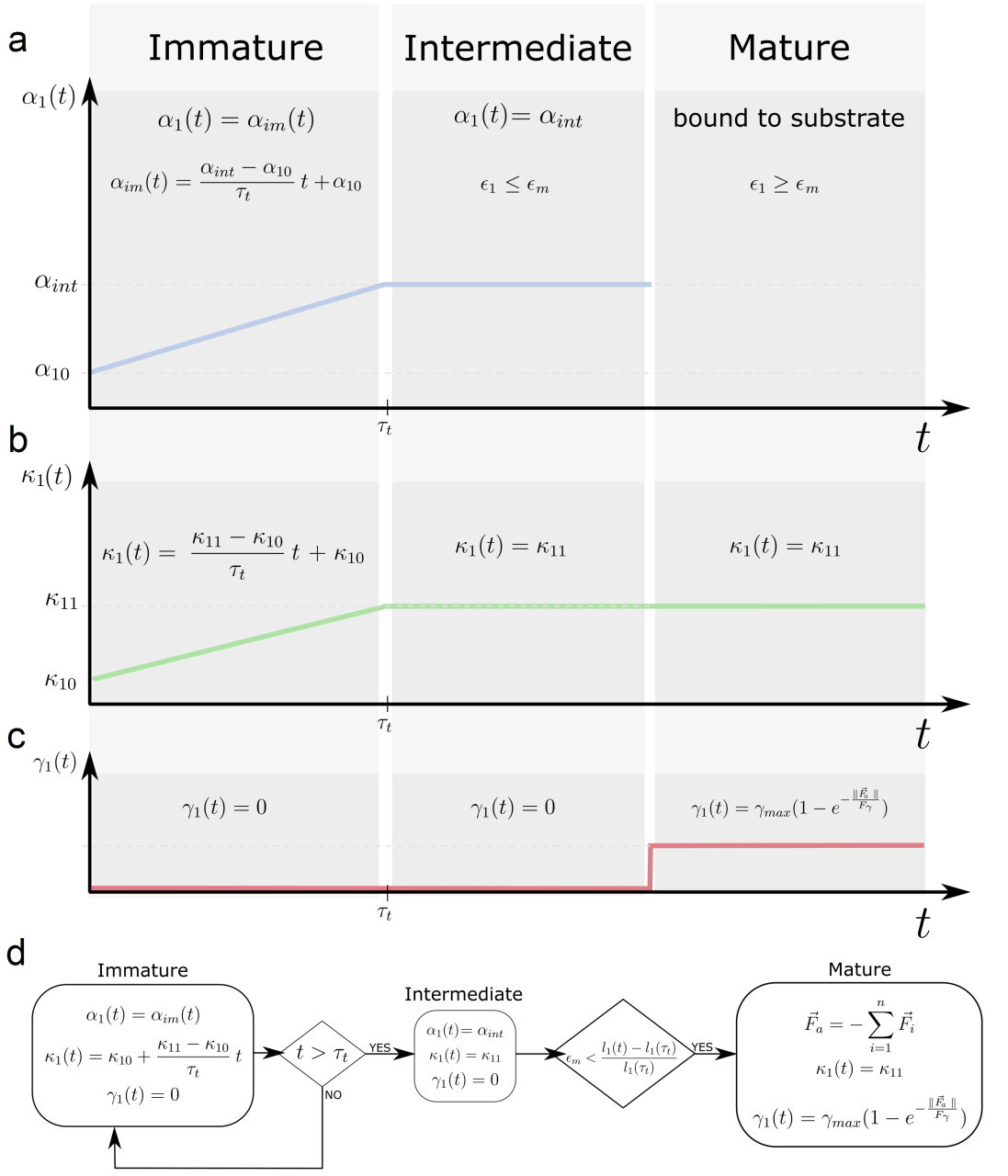

Figure 4: Summary of the evolution of the model parameters along the maturation process: (a) friction coefficient $\alpha_1(t)$, (b) branch stiffness $\kappa_1(t)$, (c) contractile force $\gamma_1(t) = F_c$, (d) associated flowchart.

2.6 Nodes disappearance

Nodes can disappear in two different ways. First they have a limited lifespan and they spontaneously disappear when this time limit is reached. The lifespan depends on the node type (see Table 1). Second the nodes that are

bound to the substrate can be broken if the total tension force exerted on the node exceeds the rupture force. In both cases, when the node disappears, the connecting branch and child nodes also disappear instantly.

3 Results

3.1 General cell behaviour

The model aims at genericity, *i.e.* at representing potentially any cell types. A particular cell type can be generated by adjusting the parameters in order to obtain a specific cell shape (from round shape to stellar shape). Specifically, changing the inhibition angle $\delta\theta_1$ for cell protrusion allows to control the number of simultaneous protrusions that a cell can generate. The size l_{10} of the B_1 branch controls the size of the actin fibres (bundles or stress fibres) that generate the protrusions. The size l_{20} of the B_2 branch controls the size of the spikes length to probe the environment. Those are lighter and more motile actin fibres (higher turnover) for faster exploration.

Figure 5 shows some examples of cell shapes that can be generated by the model by changing those parameters (a-e). Increased protrusion number and protrusion length leads to glial-like phenotypes (d), whereas suppressing the formation of actin stress fibres leads to rounder keratocyte-like phenotype (e).

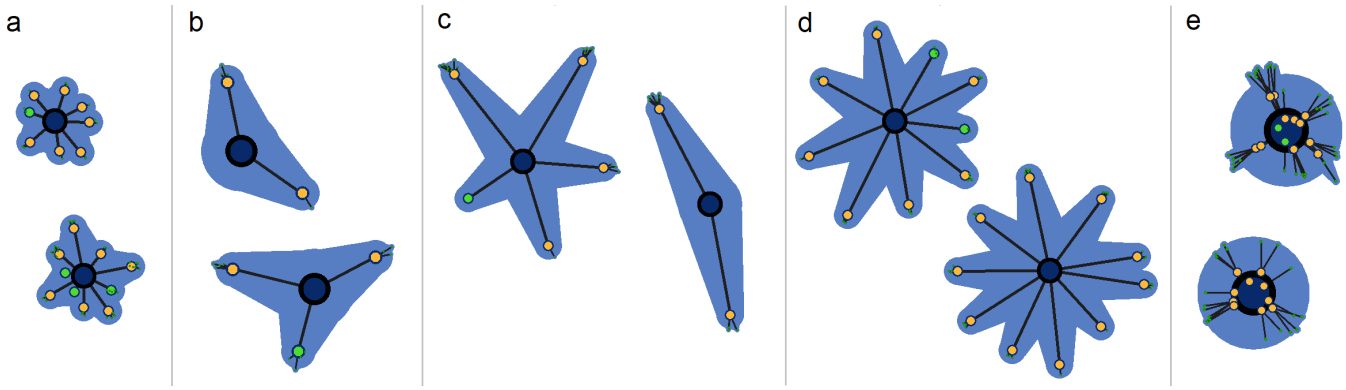

Figure 5: Examples of cell shapes that can be generated by the model by changing the inhibition angle $\delta\theta_1$ for the formation of protrusions and the initial lengths l_{10} and l_{20} of the B_1 and B_2 branches respectively. Two snapshots in a sequence of the deforming cell are presented in each case. (a) $\delta\theta_1 = \pi/6$, $l_{10} = 4\mu m$, $l_{20} = 2\mu m$; (b) $\delta\theta_1 = \pi/2$, $l_{10} = 7\mu m$, $l_{20} = 4\mu m$; (c) $\delta\theta_1 = \pi/3$, $l_{10} = 14\mu m$, $l_{20} = 4\mu m$; (d) $\delta\theta_1 = \pi/6$, $l_{10} = 14\mu m$, $l_{20} = 2\mu m$; (e) $\delta\theta_1 = \pi/6$, $l_{10} = 1\mu m$, $l_{20} = 4\mu m$.

For the simulations presented, we will consider an average unspecified cell (fig. 5.b) that we defined based on the following set of predefined constraints:

1. *cell shape:* the observation of isolated cells in two-dimensional cell culture shows that the cell shapes usually exhibit a limited number of main protrusions, rarely exceeding 4 branches (endothelial cells or fibroblasts).

We fixed this limit as a first constraint with $\delta\theta_1 = \pi/2$. The ability to form membrane spikes to probe the environment is on the other hand defined by the parameter $\delta\theta_2$. We set $\delta\theta_2 = \pi/6$ to allow a large perimeter of exploration.

2. *cell size:* the branches length, used to define B_1 and B_2, were set to match a protrusion and spike lengths respectively so that the maximum size of the cell does not exceed $50\mu m$. The values taken to remain within the values of an average cell size are $l_{10} = 7\mu m$ and $l_{20} = 4\mu m$, the latter corresponds to the length of large filopodia (Husainy et al. 2010).
3. *cell force generation:* the cell mechanical properties defined by the cell stiffness coefficients (κ) and adhesion coefficients (α) were set so that the cell can develop the required range of forces, typically around $50nN$ (Lekka et al. 2021). The progressive increase in force generation associated to the maturation of the adhesions and fibres is obtained by making these parameters evolve along the 3 maturation states.
4. *cell motile dynamics:* time parameters such as adhesion production rates (ν) and adhesion lifespans (τ) contribute to the dynamics of the cell. But more importantly, the adhesion rupture forces (F_R) and the threshold force required for cell translocation (F_{th}) determine the level of interaction of the cell with its substrate and its ability to easily detach in order to move.

A suitable set of parameters that responds to these constraints and to the admissible range of values from the literature has been determined semi-empirically (see Table 1). The simulation carried out with the above parameters is presented in figure 6.

Figure 6 shows a typical sequence of cell shape changes, in relation with the maturation of the nodes, and leading to the cell displacement. The simulation exhibits the three different outcomes for the N_1 nodes: (i) a mature node disappears and is instantly replaced by an immature node (node on the left of the cell, from *b* to *c*), (ii) a node is displaced, but the branch is not sufficiently elongated to reach the maturation criterion (node on the right of the cell, from *a* to *d*), (iii) a node progressively and successfully evolves through the three maturation stages and eventually the contraction of the mature branch leads to the cell displacement (node on the top of the cell, from *b* to *d*).

Adhesion dynamics

Cell deformations and migration have been simulated over 72 hours. The different events related to the nodes dynamics, including maturation and turnover, have been recorded. Figure 7a shows the cause of the N_1 nodes disappearance: among the 642 N_1 nodes generated, 366 (57%) disappear at the intermediate stage as their lifespan expired and 273 (43%) reach the mature state. Only 20% of the mature N_1 nodes attain their time limit, all the other

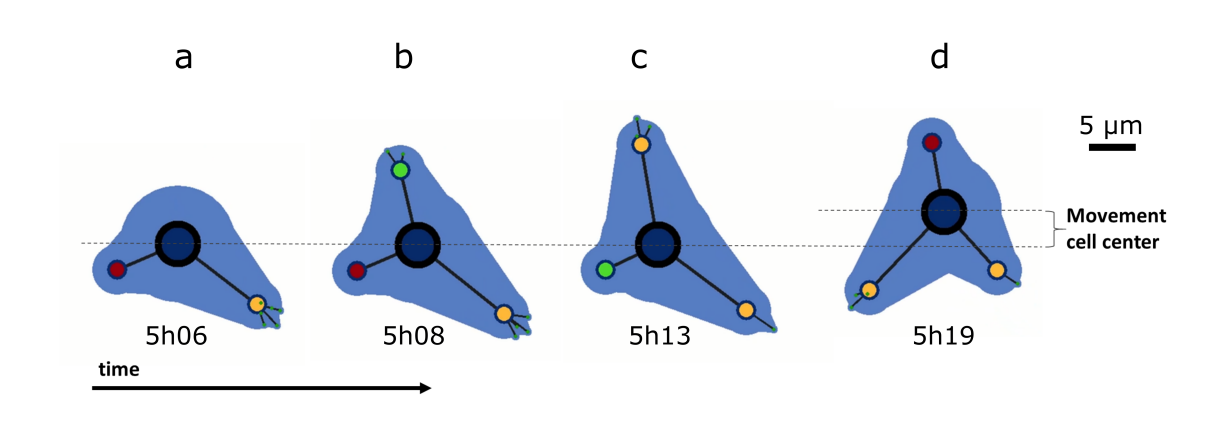

Figure 6: Cell deformation and migration observed over a 13 minute period of a long lasting simulation of 72 hours. The cell mainly exhibits a characteristic triangular shape, with dynamical movements of extension/retraction of its protrusions (branches). Colour code for N_1 node states: green for immature, yellow for intermediate and red for mature. The cell envelop in blue - made of connected circles and lines - is represented for cosmetic purpose only, since this model does not describe the cell membrane nor its cytoplasm.

mature nodes broke because of the tension forces applied on them. This relatively high contribution of the rupture force reveals that only a limited amount of mature adhesions N_1 are strong enough to resist the branch contractility as focal adhesions would. If the adhesion is strong enough to support cell translocation the cell will move, if it is not strong enough the adhesion will break (rupture). On the other hand, the main cause of death of the 8815 generated N_2 nodes is the expiration of their lifespan that accounts for 82% of the disappearances (Fig. 7b). Indeed, the role of N_2 nodes is to probe the environment dynamically. Their lifespan has been fixed short enough to favour this rapid dynamics, but long enough for the B_2 branches to exert tension forces to relocate the N_1 node in the region of interest (in the case of a heterogeneous substrate).

The maturation dynamics of the N_1 node is highlighted in figures 7c and 7d. All the 642 N_1 nodes formed during the 72 hour simulation maturate to the intermediate state since this transition is unconditional as soon as the node is 300 seconds old. At the intermediate state, the lifespan of the N_1 nodes is around 900 seconds. However, if the branch B_1 elongates sufficiently, the node maturates and this can occur over a vast period of time (as shown in fig 7d) with an average time of $233 \pm 139s$, *i.e.* well before reaching the lifespan limit. This ensures that a sufficient amount (about 43%) of N_1 nodes will maturate. Once maturation is reached, an enhanced force competition - with the addition of a contractile force component - takes place in the branch. Rupture of the N_1 nodes occurs on a relatively short window period of $95 \pm 96s$ after the node reaches maturation. The remaining nodes reach their time limit of about 2000 seconds.

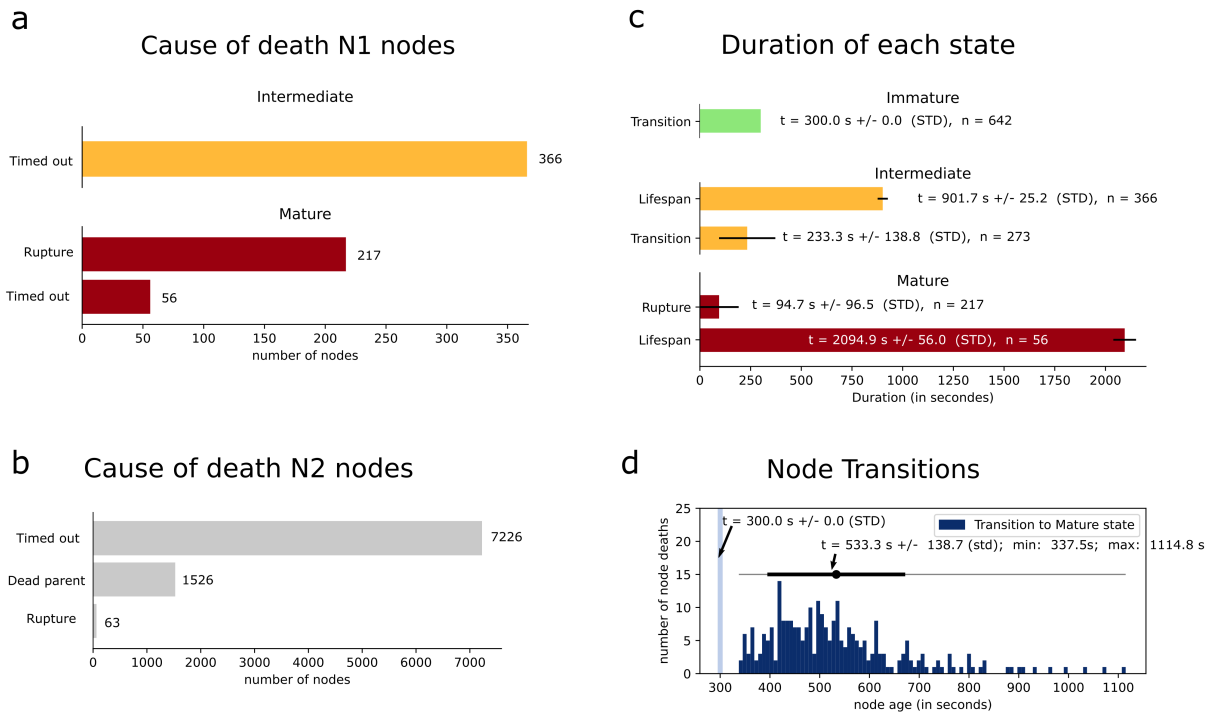

Figure 7: Nodes dynamics for a single cell over a 72 hour simulation. (a) cause of death for the intermediate and mature N_1 nodes; (b) cause of death of the N_2 nodes; (c) duration at which the transitions to the more mature states occur, effective durations of the nodes lifespan and mean duration at which a mature node breaks (STD stands for standard deviation of the mean); (d) recorded N_1 node transition events in function of the node age. All immature to intermediate transitions happened at the age of 300s, while all intermediate to mature transitions happened afterwards. The horizontal grey line spans from the earliest to the latest transition, while the black spot and bar show mean transition age and its standard deviation. We note that the node age is the sum of the times spent in each state. Colour code for N_1 node states: green for immature, yellow for intermediate and red for mature.

Force generation

Adhesions and branches mature concomitantly. The maturation of the branch is characterized by the progressive increase of the force it can generate on its nodes. Figure 8 displays the evolution of the forces generated in the branches and exerted on the nodes during a sequence of a single cell movement of about one hour in order to highlight how the forces in the branches drive the nodes displacement dynamics and cell migration. In figure 8, the upper graph shows that at the immature stage, the forces in the B_1 branches remain very small despite the linear increase of the elasticity coefficient with time. After 300s the elasticity coefficient of the branch stops evolving and the branch resting length is redefined to its acquired length. These new conditions define the intermediate state of the branch where the force progressively increases, often above 20nN, because of the branch elongation due to the N_1 node displacement under the traction of the B_2 branches (not represented). If the B_1 branch elongation reaches the elongation threshold ε_m then the B_1 branch attains the mature state and becomes contractile. This acquired contractility generates a jump of about 40nN in the branch force. This value was defined so as to generate a level of force on N_0 sufficiently high to displace this node, *i.e.* for the cell to migrate. In figure 8, the lower graph shows the resulting forces applied by the branches on the nodes. Forces applied on the N_1 nodes appear as a succession of spikes of about 20nN in intensity. This spike profile is explained by the N_1 node displacement that dissipates the resulting force from the B_1 and B_2 branches. Force dissipation is possible as long as N_1 is free to move, *i.e.* when it is in its immature or intermediate states. At the mature state, the N_1 node is bounded to the substrate to resist the contractile force. If the force on the node reaches the threshold F_{R1} then the node breaks and instantly dissipates the force (two occurrences for node 1 and node 5 in the figure). In both cases the sudden force increase in the branch is sufficient to reach the threshold force F_{th} on the N_0 node required for the cell to move (*i.e.* non-zero speed) just before the times 750s and 2000s. All other cases of cell displacements (*i.e.* non-zero speed) occurred when at least one branch became contractile to increase the resulting force on the N_0 node above the F_{th} threshold.

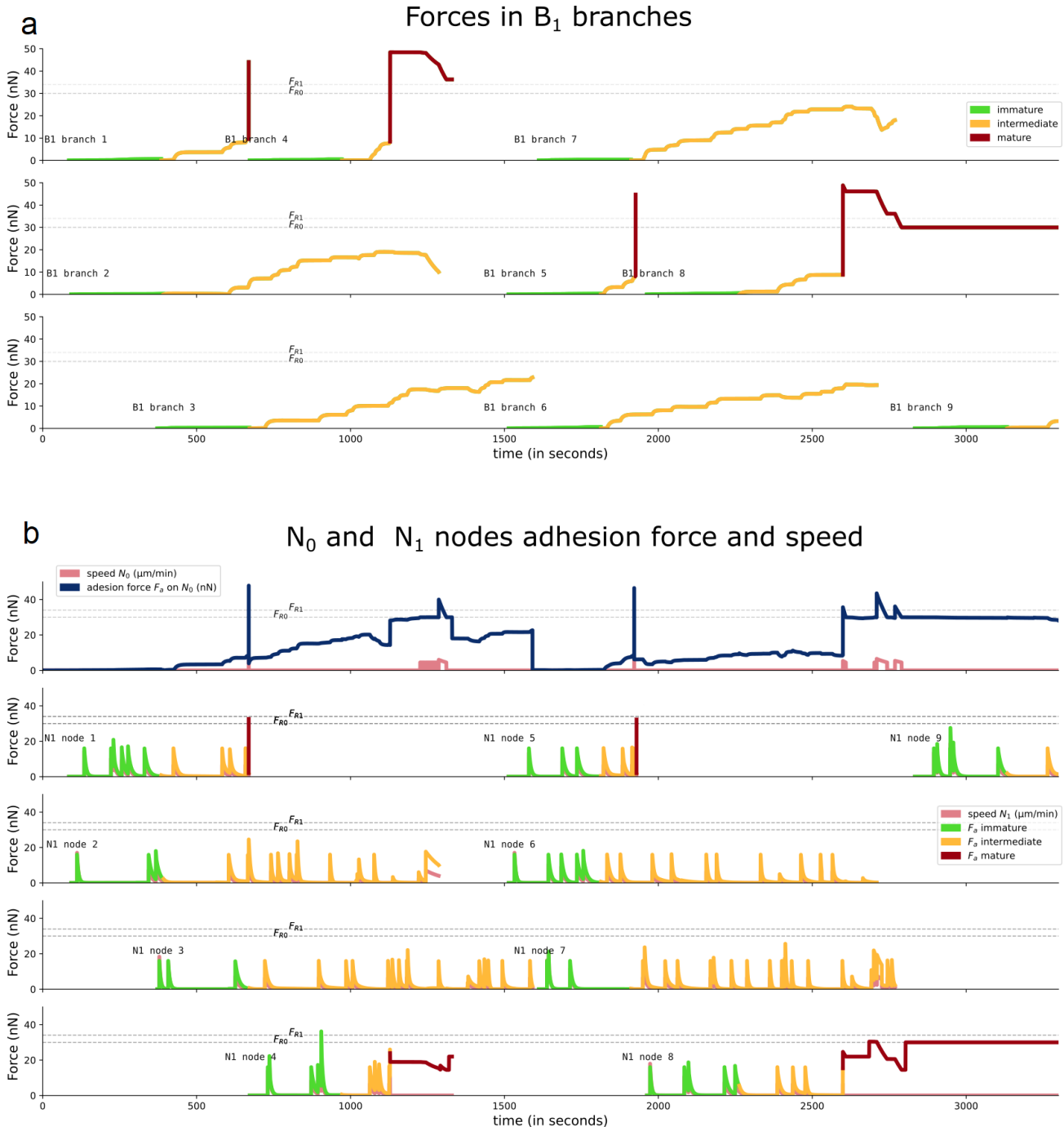

Figure 8: Upper graph (a): evolution of the force intensity in the different B_1 branches. The branches are displayed on 3 graphs to avoid overlapping of the co-existing branches. During the one-hour observation period 9 branches are observed with in average 3 co-existing branches. The colour code represents the maturation state of the branch: immature (green), intermediate (yellow), mature (red). Lower graph (b): evolution of the intensity of the resulting forces applied on the N_0 (first row) and N_1 nodes (rows 2 to 4). The N_1 nodes are displayed on 4 graphs to avoid overlapping of the co-existing nodes. During the one-hour observation period 9, N_1 nodes were observed. The colour code represents the maturation state of the N_1 node: immature (green), intermediate (yellow), mature (red). The horizontal grey dotted lines in each graph represent the force thresholds $F_{R0} = F_{th}$ for N_0 to move and F_{R1} for N_1 to break.

3.2 Cell migration on a homogeneous substrate

To test the model we first perform cell migration simulations on a homogeneous substrate. Figure 9 (upper left graph) presents the superimpositions of 50 single cell trajectories recorded over 72 hours. The homogeneous distribution of the trajectories is coherent with a typical random migration behaviour, meaning that our model does not introduce any migration bias. We then tested the influence of the attachment force of the cell to the substrate. The cell attachment force corresponds to the threshold forces triplet (F_{th}, F_{R1}, F_{R2}) that can change depending on the biochemical nature of the substrate, *i.e.* on the cell matrix fibres composition, characterized by the amount of ligands and/or the strength of the adhesive bonds with which the cell can interact. To change the cell-substrate affinity, *i.e.* the cell attachment force, we introduce the dimensionless parameter δ to modulate the force magnitude as $\delta \times (F_{th}, F_{R1}, F_{R2}) = (\delta F_{th}, \delta F_{R1}, \delta F_{R2})$. We then compare $\delta = 1$ which is the reference simulation with $\delta = 1.5$ which means a 50% increase of the attachment force. Figure 9 (upper right graph) shows that the cell exploration zone is significantly reduced while maintaining its random migration characteristic.

If δ is changed from 0.25 to 2.0, the average cell speed evolves with a bell shape (Fig.9, lower graph) which is in agreement with experimental facts (Palecek et al. 1997). For $\delta < 1$ the cell remains unable to move since the attachment force is too weak for the cell to adhere to the substrate. The level of forces developed by the branches systematically break the adhesions that cannot strengthen and reach maturation to allow the cell to move. Once the attachment force is strong enough for $\delta \geq 1$ then the cell can move. For $\delta = 1.125$ the average cell speed reaches its maximum close to $8\mu m/h$, and decreases progressively for increasing values of δ. When the attachment force is higher, then the cell adhesions reach maturation however the forces developed in the branches are not high enough to reach the cell translocation threshold which limits the cell migration.

Since the level of force for cell translocation can only be reached once the N_1 adhesion is mature, we further tested the influence of the mature N_1 adhesion lifespan τ_m (Fig.9, lower graph). As expected, when the adhesion lifespan is shorter $(\tau_m/2 = 17min)$, there is a higher turnover of the adhesions which allows the cell to move more often, thus increasing the average migration speed. On the other hand when the lifespan is longer $(2 \times \tau_m = 70min)$, then the cell adhesion and its associated branch which does not reach the translocation threshold force remains stuck until the adhesion is released as it reaches its time limit. This is slowing down the cell migration speed. In the extreme case where the adhesion lifespan τ_m is infinite, the only way to break the adhesion is for the associated branch to reach the translocation threshold. The lack of adhesion turnover reduces drastically the average migration speed by a factor two (the maximum speed is $4\mu m/h$), however the cell remains able to migrate.

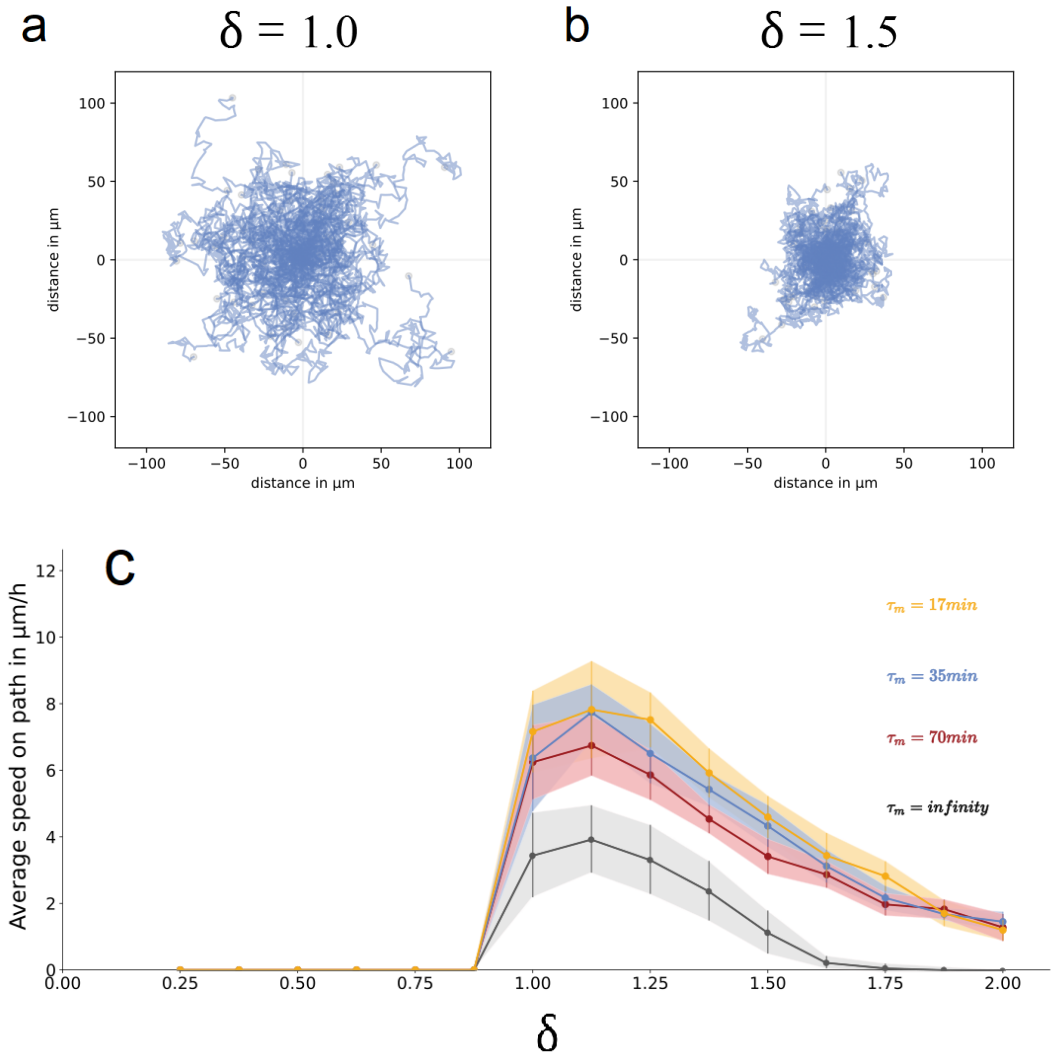

Figure 9: Upper graphs: Cell trajectories on a homogeneous substrate for two cell detachment conditions $\delta = 1.0$ (a) and $\delta = 1.5$ (b). Fifty trajectories of a single cell moving for 72 hours are superimposed in each graph. Lower graph (c): Average cell speeds as a function of the parameter δ representing the cell detachment condition. Each point of the curves corresponds to 10 trajectories of a single cell moving for 12 hours. Each coloured curve corresponds to a different value for τ_m, the lifespan of mature N_1 nodes. $\tau_m = 35$ min is the reference simulation used in the two upper graphs.

3.3 Constrained cell migration on adhesive patterns

Engineered adhesive patterns, typically coated with fibronectin, are often used to constrain the cell shape in order to study the resulting cytoskeletal organization. They can also be used to investigate the factors influencing the cell displacements. Inspired by the study of Lo Vecchio et al. (2020), we challenged our cell model by constraining the cell migration on a stripe of adhesive triangular patterns. By varying pattern spacing, the aim was to determine if the pattern can favour a migration direction on our virtual cell. The triangular shape presents an adhesive asymmetry for the cell surface adherence between the left and the right side of the patterns. The question is *will the cell follow the arrows ?*

For the simulations, the nodes N_1 and N_2 can only form if in contact with the pattern. Each triangle of the pattern is $10\mu m$ high and $20\mu m$ long (Fig. 10). The gap distance between consecutive triangles is set for each simulation. It varies from -$12\mu m$ to $4\mu m$ with an increment of $4\mu m$ from one simulation to another. A negative value of the gap distance means that the triangles overlap with this length. We also considered a pattern of reference with no bias, corresponding to a continuous adhesive stripe.

Figure 10 (left) exhibits a sequence of cell movements and displacements on the adhesive pattern with a gap distance between consecutive triangles that is equal to zero. The cell forms branches that can reach the triangles on the left or on the right. However the inhibition condition for node and branch formation implemented in the model (see Fig. 2), limits the formation of a single branch per triangle (the triangle is not big enough to accommodate two N_1 nodes). As a consequence, the direction for the cell displacement is not the resultant of the force competition between left and right, since the forces tend to equilibrate with one branch on each side. On the other hand it mostly depends on the probability to form some adhesions, which is directly related to the differential length of the arcs corresponding to the intersection of the circle of radius l_{01} with the adhesive surface at each side of the cell. This is a strong difference with the experiments of Lo Vecchio *et al.* (2020) where the differential quantities between both sides of the cell is the adhesion area. Indeed the longer the arcs does not mean/correspond to the largest adhesion area.

To compare our theoretical results with the experimental results of Lo Vecchio *et al.* (2020) we used the same representation where the respective percentage of cells ending their trajectories on the left (-) or right side (+) from their initial position is plotted as a function of the gap distance between the triangular patterns (Fig. 11.a). As in the experiments, the bias towards the positive direction tends to increase with the gap distance. But whereas in the experiments, the negative direction is selected for small gap distances, it is never the case in our simulations. The

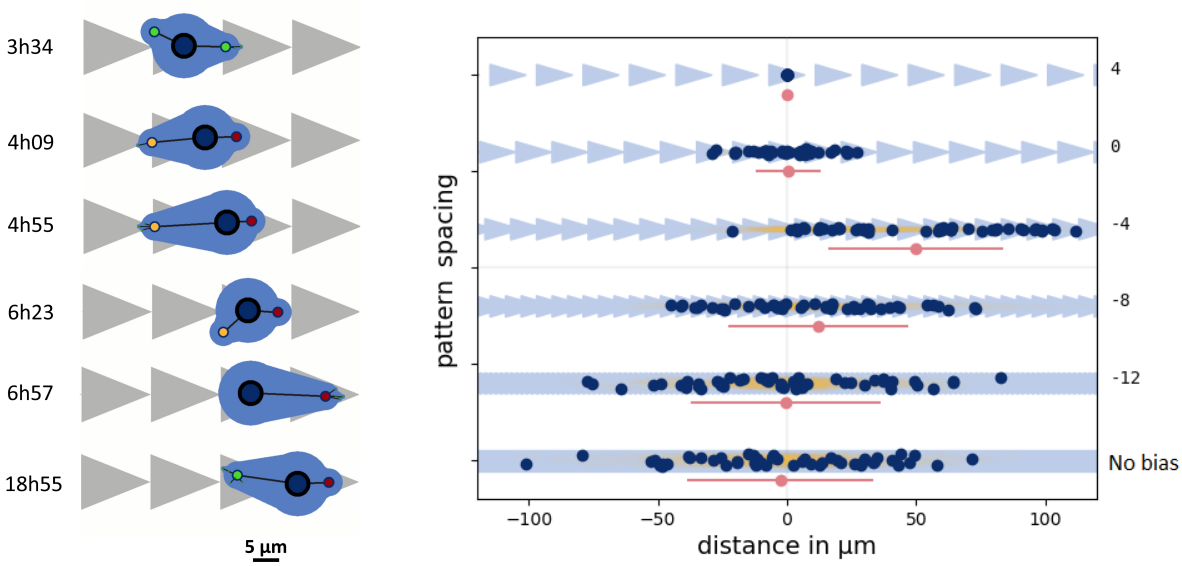

Figure 10: Left graph: cell displacement on triangular adhesive patterns. Right graph: each single cell was left to move on the pattern and its position after 72 hours is represented by a dark blue dot. The positions of 50 cells are displayed for each pattern spacing value. The average position and standard mean displacement are respectively represented by a red dot and line. The simulations are reproduced for different triangular pattern spacing from $4\mu m$ until there is a continuous adhesive strip (meaning no direction bias).

main reason is that our model is less sensitive to the substrate since, as explained above, the N_1 nodes form at a fixed distance from the cell centre and do not exploit the whole adhesion area available.

To quantify the cell migration properties, Lo Vecchio et al. (2020) proposed the calculation of a coefficient p informing on the direction bias of the cell trajectory. This coefficient is calculated from the quantities N_+ and N_- that correspond respectively to the number of steps made by the cell in the positive direction (following the tips of the triangles) N_+ and in the negative direction (opposite direction) N_- during a 48 hour sequence of migration:

$$p = \frac{N_+ - N_-}{N_+ + N_-} \tag{15}$$

The difference with the previous graph is that all the migration steps are exploited and not just the terminal position of the cell (Fig 11.b). The figure confirms that the bias increases with the gap distance, whereas in the experiments the increase is initially small and gets bigger with the gap distance, our simulations show the opposite with an initially high increase that saturates. Again this is due to the fact that experimentally the cell is able to stretch itself to attain the next distant pattern. In the model the protrusion is emitted at a constant length hence there is a saturation effect.

As a consequence, the model is qualitatively valid but is not refined enough to be quantitatively accurate. The limitation related to the constant length of emitted protrusions, can however be easily addressed by allowing the formation of N_1 nodes at distances from the cell centre determined by a normal distribution in a future implementation of the model.

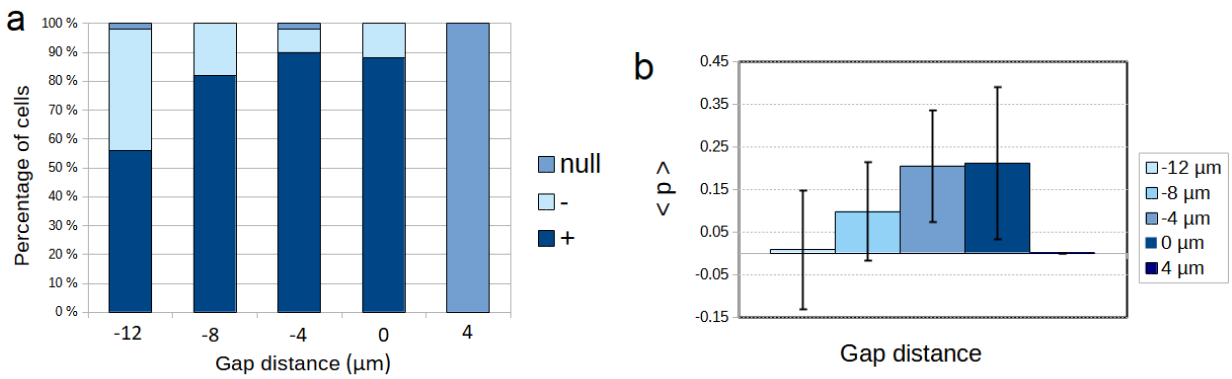

Figure 11: Left graph (a): percentage of cells ending their trajectories in the left side (-), right side (+) or same position (null) from their initial position, as a function of the gap distance. Right graph (b): average direction bias of the cell trajectories ($< p >$) as a function of the gap distance. Measurements in both graphs were made from 50 cells migrating for 48 hours.

4 Discussion

The model developed was aimed to address cell sensing of the substrate and how this influences cell migration dynamics. The model was designed to be generic enough in order to be adjusted to match the characteristics of a large variety of cell types in terms of morphology and migration velocity. It can thus potentially describe any type of cell including fibroblasts, macrophages, keratocytes, glial cells and can also be tuned to match tumor cells.

For this, a number of key parameters need to be defined. The model was designed so as to keep the number of parameters as small as possible, by identifying dependencies between the parameters of a same type (temporal parameters, force parameters, *etc.*) It is then relatively easy, to determine the parameters in a semi-empirical way, based on the admissible range of values from the literature and on a set of observables that defines the cell type of interest.

In the simulations presented we chose to model an unspecified cell to better highlight the full model potential. The structural and mechanical model parameters were defined based on the following observables that are used as model constraints : (1) the cell size should not exceed $50\mu m$; (2) the number of cell branches was limited to 4; (3) the fibres elasticity coefficient and adhesion coefficient were set so that the cell can develop a range of forces

around $50nN$; (4) the adhesion lifespans and rupture forces depend on the interaction of the cell with its substrate. They were determined so that the cell dynamical behaviour is compatible with available experimental observations regarding the cell velocity.

The first two constraints determine the cell morphology. The size is set by the branch length parameters, and the shape by the exclusion angle between branches. If the exclusion angle is large, the branches formed will be spaced and the cell will take a more starlike shape compatible with glial cells or fibroblasts. On the other hand if the exclusion angle is small the cell will have a more rounded shape compatible with keratocytes for example. The third and fourth constraints defined the adhesion turnover, i.e. the cell dynamics where the migration velocity highly depends on the nature of the substrate (adhesivity and rigidity in our example).

The cell model was first tested by considering a homogeneous substrate. As expected, no directional bias was observed. However, the adhesion conditions clearly impacted the cell movements. More specifically the adhesion velocity evolves with the increase of the adhesion strength in a biphasic manner, thus reproducing the well known experimental bell-shape curve (Palecek et al. 1997). The velocity first increases with the adhesion strength to reach an optimum above which the cell migration is refrained. We showed that this is additionally modulated by the adhesion lifespan (τ_m). This needs to be finely tuned so that maturation has time to develop while ensuring adequate adhesion turnover.

The model was then challenged with a non-homogeneous substrate based on the experiments by Lo Vecchio et al. (2020) that uses asymmetrical adhesive patterns. As in the experiments, the model reproduces the observed migration bias. However quantitative differences were obtained and exhibit some model limitations. Indeed in the current model implementation, the cell protrusions (branches) are emitted with a constant length that do not allow to explore the entire adhesive surface offered to the cell. However this limitation can easily be addressed by relaxing this condition and by defining the branch length in a normal distribution.

The strength of the model resides in its simplicity which allows to describe a wide range of cell morphologies and dynamics in relation with the environmental properties thanks to the implementation of cell sensing. The dynamic nature of the probing filopods associated to the maturation of focal adhesions makes this model particularly well adapted to explore further the cell-matrix interactions through more complex coupling including matrix rigidity gradient, deformable visco-elastic matrices, anisotropic matrix topography through matrix fibre orientations, *etc*. Moreover the model was designed to be easily generalizable in 3D. Structurally, this only requires the addition of an azimuthal angle to define the branch position in the 3D space. Cell migration in a 3D environment requires the cell to move through a dense network of fibres. In order to overcome the steric hindrance, the cell can either squeeze through the pores of the matrix network, or degrade the matrix to create the space needed for its migration. Our model can easily address cell squeezing since the only physical part of the cell in the model is the cell nucleus, the

membrane is not explicitely described. The deformation of the nucleus from a sphere to an ellipsoid of equivalent volume is straigthforward and only involves setting a threshold for the allowed deformation associated with the mechanical properties of the nucleus, as a first approximation. Regarding matrix degradation, the cell secretion of matrix degrading enzymes such as matrix metalloproteases (MMPs) and their diffusion are necessary. This implies including a partial differential equation to address this aspect, which we have already considered in a previous 2D model (Stéphanou et al. 2015).

In its current implementation the model allows for fast simulations. One hour of a single cell computation is performed in 0.2 second without visualization. The biggest performance hits were caused by recording the amount of data onto the disk. However this can be optimized. In addition, parallel optimization could be further implemented to process high cell count simulations in real time or even faster. The recorded computation speed suggests that the model could be implemented to study various multi-cellular phenomena such as morphogenesis, tissue patterning and angiogenesis, which were previously performed via grid dependent modelling schemes. These simulations could therefore include a few hundred or even a few thousand cells, while delivering results within a reasonable time frame. In addition, the simplicity of the modelling paradigm makes it flexible enough to be adapted to various scenarii, which makes it a promising modelling framework for the future.

Parameter	Description	Value	unit	Ref.
Cell shape				
$\delta\theta_1$	inhibition angle for N_1	$\pi/2$	-	
$\delta\theta_2$	apparition angle for N_2	$\pi/6$	-	
l_{10}	initial length of B_1	7	μm	
l_{20}	initial length of B_2	4	μm	
Adhesion dynamics				
ν_1	production rate of N_1	0.01	s^{-1}	(1)
ν_{2im}	production rate of N_2 from immature N_1	0.015	s^{-1}	
ν_{2int}	production rate of N_2 from intermediate N_1	0.015	s^{-1}	
ν_{2m}	production rate of N_2 from mature N_1	0.00001	s^{-1}	
τ_t	duration of N_1 immature state	5	*min*	
τ_{int}	lifespan of intermediate N_1	15	*min*	
τ_m	lifespan of mature N_1	35	*min*	(2)
τ_2	lifespan of N_2	200	*s*	
Substrate interaction				
α_0	friction coefficient of N_0	400	$nN \cdot s/\mu m$	
α_{10}	initial friction coefficient of N_1	50	$nN \cdot s/\mu m$	
α_{int}	friction coefficient of intermediate N_1	150	$nN \cdot s/\mu m$	
α_m	friction coefficient of mature N_1	165	$nN \cdot s/\mu m$	
α_2	friction coefficient of N_2	8	$nN \cdot s/\mu m$	
F_{th}	Threshold force for N_0 displacement	30	*nN*	(3)
F_{R1}	Rupture force of N_1	34	*nN*	
F_{R2}	Rupture force of N_2	17	*nN*	
Actin branch property				
ε_m	maturation Cauchy strain of B_1	0.5	-	
ε_{20}	initial Cauchy strain of B_2	0	-	
κ_{10}	initial stiffness of B_1	0.1	$nN/\mu m$	
κ_{11}	stiffness of B_1	3.5	$nN/\mu m$	(1)
κ_2	stiffness of B_2	12	$nN/\mu m$	
γ_{max}	contractility of B_1	40	*nN*	(4)
F_γ	force constant	30	*nN*	

Table 1: Model parameters. Cell shape parameters: $\delta\theta_1$ and $\delta\theta_2$ allow to define the maximum number of cell protrusions and the width of the exploration area by the filopods respectively; $l_{10} + l_{20}$ define the maximum length of the cell membrane extension. The adhesion dynamics is defined from the production rates ν and lifespans τ of each adhesion types. They are hierarchically define depending on the adhesion type and maturation level. Since the extracellular matrix is not explicitly represented, the cell interaction with the substrate is defined through the friction coefficients α and rupture forces F. The actin branch properties are defined by the Cauchy strains ε, stiffnesses κ and contractility γ. The parameter values have been semi-empirically defined to generate a given cell shape and migration dynamics in agreement with range of values from the literature: (1) Zhu & Mogilner (2016); (2) Stehbens & Wittmann (2014), Oakes & Gardel (2014); (3) Lekka et al. (2021); (4) Boys & Owens (2021).

Declarations

Ethical Approval

Not applicable.

Competing interests

Not applicable.

Authors' contributions

All authors contributed in the model development. I.M. made the simulations and prepared the figures. A.S. wrote the manuscript. A.C., C.V., G.C. and I.C. reviewed the manuscript.

Funding

This work was supported by the LabEx PERSYVAL-Lab (ANR-11-LABX-0025-01) funded by the French program Investissements d'Avenir. It also received funding from PEPS CNRS - INSIS "La mécanique du futur" (2021). C.V. is a member of the labex Tec21 (ANR-11-LABX-0030) funded by the French program Investissements d'Avenir.

Acknowledgements

We thank Benjamin Girard and Arnold Fertin for reshaping the code and making it more user friendly.

Availability of data and materials

The code is publicly available at the following GitLab repository :

`https://gricad-gitlab.univ-grenoble-alpes.fr/stephana/cell-motility`

References

Abercrombie, M. (1980), 'The crawling movement of metazoan cells', *Proc. R. Soc. Lond.* **207**(1167), 129–47.

Abercrombie, M., Heaysman, J. & Pegrum, S. (1970), 'The locomotion of fibroblasts in culture. i. movements of the leading edge', *Experimental Cell Research* **59**(3), 393–8.

Akbarzadeh Solbu, A., Caballero, D., Damigos, S., Kundu, S. C., Reis, R. L., Halaas, O., Chahal, A. S. & Strand, B. L. (2023), 'Assessing cell migration in hydrogels: an overview of relevant materials and methods', *Materials Today Bio* **18**, 100537.

Bangasser, B., Shamsan, G., Chan, C., Opoku, K., Tüzel, E., Schlichtmann, B., Kasim, J., Fuller, B., McCullough, B., Rosenfeld, S. & Odde, D. (2017), 'Shifting the optimal stiffness for cell migration', *Nat Commun* **8**, 15313.

Bouchalova, P. & Bouchal, P. (2022), 'Current methods for studying metastatic potential of tumor cells', *Cancer Cell Int.* **22**(1), 394.

Boys, A. & Owens, R. (2021), 'Measuring cellular contraction: Current progress and a future in bioelectronics', *APL Mater* **9**(4), 040903.

Caballero, D., Voituriez, R. & Riveline, D. (2014), 'Protrusion fluctuations direct cell motion', *Biophysical Journal* **107**(1), 34–42.

Chandra, A., Butler, M. T., Bear, J. E. & Haugh, J. M. (2022), 'Modelling cell protrusion predicts how myosin ii and actin turnover affect adhesion-based signaling', *Biophysical Journal* **121**, 102–118.

Chi, Q., Yin, T., Gregersen, H., Deng, X., Fan, Y., Zhao, J., Liao, D. & Wang, G. (2014), 'Rear actomyosin contractility-driven directional cell migration in three-dimensional matrices: a mechano-chemical coupling mechanism.', *J R Soc Interface* **11**(95), 20131072.

Eichinger, J. F., Grill, M. J., Davoodi Kermani, I., Aydin, R. C., Wall, W. A., Humphrey, J. D. & Cyron, C. J. (2021), 'A computational framework for modelling cell-matrix interactions in soft biological tissues', *Biomechanics and Modeling in Mechanobiology* **20**, 1851–70.

Franco, C., Tzvetkova-Chevolleau, T. & Stéphanou, A. (2010), 'On the influence of discrete adhesive patterns for cell shape and motility: a computational approach', *Mathematical Modelling of Natural Phenomena* **5**(1).

Galbraith, C. G., Yamada, K. M. & Galbraith, J. A. (2007), 'Polymerizing actin fibers position integrins primed to probe for adhesion sites.', *Science* **315**(5814), 992–995.

Gardel, M. L., Sabass, B., Ji, L., Danuser, G., Schwarz, U. S. & Waterman, C. M. (2008), 'Traction stress in focal adhesions correlates biphasically with actin retrograde flow speed.', *J Cell Biol* **183**(6), 999–1005.

Garner, R. M. & Theriot, J. A. (2022), 'Leading edge maintenance in migrating cells is an emergent property of branched actin network growth', *Elife* **11**, e74389.

Heck, T., Vargas, D., Smeets, B., Ramon, H., Van Liedekerke, P. & Van Oosterwyck, H. (2020), 'The role of actin protrusion dynamics in cell migration through a degradable viscoelastic extracellular matrix: Insights from a computational model', *PLoS Comput Biol* **16**(1), e1007250.

Holmes, W. R., Golding, A. E., Bement, W. M. & Edelstein-Keshet, L. (2016), 'A mathematical model of gtpase pattern formation during single-cell wound repair', *Interface Focus* **6**(5), 20160032.

Husainy, A. N., Morrow, A. A., Perkins, T. J. & Lee, J. M. (2010), 'Robust patterns in the stochastic organization of filopodia', *BMC Cell Biology* **11**(1).

Isomursu, A., Park, K., Hou, J., Cheng, B., Mathieu, M., Shamsan, G., ... & Odde, D. J. (2022), 'Directed cell migration towards softer environments', *Nat Mater* **21**(9), 1081–1090.

Kim, M.-C., Neal, D., Kamm, R. & Asada, H. (2013), 'Dynamic modeling of cell migration and spreading behaviors on fibronectin coated planar substrates and micropatterned geometries', *PLoS Comput Biol* **9**(2), e1002926.

Kim, M.-C., Silberberg, Y., Abeyaratne, R., Kamm, R. & Asada, H. (2018), 'Computational modeling of three-dimensional ecmrigidity sensing to guide directed cell migration', *PNAS* **115**(3), E390–E399.

Kim, M.-C., Whisler, J., Silberberg, Y., Kamm, R. & Asada, H. (2015), 'Cell invasion dynamics into a three dimensional extracellular matrix fibre network', *PLoS Comput Biol* **11**(10), e1004535.

Kruse, K., Joanny, J. F., Jülicher, F. & Prost, J. (2006), 'Contractility and retrograde flow in lamellipodium motion.', *Phys Biol* **3**(2), 130–137.

Kulesa, P. M., Kasemeier-Kulesa, J. C., Morrison, J. A., McLennan, R., McKinney, M. C. & Bailey, C. (2021), 'Modelling cell invasion: a review of what jd murray and the embryo can teach us', *Bulletin of Mathematical Biology* **83**(26).

Legerstee, K. & Houtsmuller, A. B. (2021), 'A layered view on focal adhesions', *Biology* **10**(11), 1189.

Lekka, M., Gnanachandran, K., Kubiak, A., Zielinski, T. & J, Z. (2021), 'Traction force microscopy - measuring the forces exerted by cells', *Micron* **150**, 103138.

Liu, Y.-J., Berre, M. L., Lautenschlaeger, F., Maiuri, P., Callan-Jones, A., Heuzé, M., Takaki, T., Voituriez, R. & Piel, M. (2015), 'Confinement and low adhesion induce fast amoeboid migration of slow mesenchymal cells.', *Cell* **160**(4), 659–672.

Lo Vecchio, S., Thiagarajan, R., Caballero, D., Vigon, V., Navoret, L., Voituriez, R. & Riveline, D. (2020), 'Collective dynamics of focal adhesions regulate direction of cell motion', *Cell Systems* **10**(6), 535–542.e4.

Marée, A. F., Jilkine, A., Dawes, A., Grieneisen, V. A. & Edelstein-Keshet, L. (2006), 'Polarization and movement of keratocytes: a multiscale modelling approach', *Bulletin of Mathematical Biology* **68**, 1169–1211.

Mavrakis, M. & Juanes, M. (2023), 'The compass to follow: Focal adhesion turnover', *Curr Opin Cell Biol* **80**, 102152.

Merino-Casallo, F., Gomez-Benito, M. J., Martinez-Cantin, R. & Garcia-Aznar, J. M. (2022), 'A mechanistic protrusive-based model for 3d cell migration', *European Journal of Cell Biology* **101**(3), 151255.

Muntz, I., Fenu, M., Osch, G. J. & Koenderink, G. H. (2022), 'The role of cell-matrix interactions in connective tissue mechanics', *Physical Biology* **19**, 021001.

Oakes, P. & Gardel, M. (2014), 'Stressing the limits of focal adhesion mechanosensitivity', *Curr Opin Cell Biol* **30**, 68–73.

Palecek, S. P., Loftus, J. C., Ginsberg, M. H., Lauffenburger, D. A. & Horwitz, A. F. (1997), 'Integrin-ligand binding properties govern cell migration speed through cell-substratum adhesiveness', *Nature* **385**(6616), 537–540.

Parsons, J. T., Horwitz, A. R. & Schwartz, M. A. (2010), 'Cell adhesion: integrating cytoskeletal dynamics and cellular tension', *Nature Reviews Molecular Cell Biology* **11**(9), 633–643.

Peschetola, V., Laurent, V. M., Duperray, A., Michel, R., Ambrosi, D., Preziosi, L. & Verdier, C. (2013), 'Time-dependent traction force microscopy for cancer cells as a measure of invasiveness.', *Cytoskeleton* **70**(4), 201–214.

Petrie, R. J., Koo, H. & Yamada, K. M. (2014), 'Generation of compartmentalized pressure by a nuclear piston governs cell motility in a 3d matrix', *Science* **345**(6200), 1062–1065.

Reinhardt, J., Krakauer, D. & Gooch, K. (2013), 'Complex matrix remodeling and durotaxis can emerge from simple rules for cell-matrix interaction in agent-based models', *Journal of Biomechanical Engineering* **135**, 071003.

Rens, E. G. & Edelstein-Keshet, L. (2019), 'From energy to cellular forces in the cellular potts model: an algorithmic approach', *PLoS Computational Biology* **15**(12), e1007459.

Rens, E. & Merks, R. (2020), 'Cell shape and durotaxis explained from cell-extracellular matrix forces and focal adhesion dynamics', *iScience* **23**, 101488.

Satulovsky, J., Lui, R. & Wang, Y. (2008), 'Exploring the control circuit of cell migration by mathematical modeling', *Biophys J* **94**, 3671–3683.

Schluter, D., Ramis-Conde, I. & Chaplain, M. (2012), 'Computational modeling of single-cell migration: The leading role of extracellular matrix fibers', *Biophys J* **103**, 1141–1151.

Starke, J., Maaser, K., Wehrle-Haller, B. & Friedl, P. (2013), 'Mechanotransduction of mesenchymal melanoma cell invasion into 3d collagen lattices: Filopod-mediated extension-relaxation cycles and force anisotropy.', *Exp Cell Res* **319**(16), 2424–2433.

Stehbens, S. & Wittmann, T. (2014), 'Analysis of focal adhesion turnover: A quantitative live cell imaging example', *Methods Cell Biol* **123**, 335–346.

Stéphanou, A. (2009), A computational framework integrating cytoskeletal and adhesion dynamics for modelling cell motility, *in* A. Chauvière, L. Preziosi & C. Verdier, eds, 'Cell mechanics, from single scale-based models to multiscale modeling', Chapman & Hall CRC Press, pp. 91–112.

Stéphanou, A., Le Floc'h, S. & Chauvière, A. (2015), 'A Hybrid Model to Test the Importance of Mechanical Cues Driving Cell Migration in Angiogenesis', *Mathematical Modelling of Natural Phenomena* **10**(1), 142–166.

Stéphanou, A., Mylona, E., Chaplain, M. & Tracqui, P. (2008), 'A computational model of cell migration coupling the growth of focal adhesions with oscillatory cell protrusions', *Journal of Theoretical Biology* **253**(4), 701–716.

Theriot, J. A. & Mitchison, T. J. (1991), 'Actin microfilament dynamics in locomoting cells', *Nature* **352**(6331), 126–31.

Vernerey, F. J. & Farsad, M. (2014), 'A mathematical model of the coupled mechanisms of cell adhesion, contraction and spreading', *Journal of Mathematical Biology* **68**(4), 989–1022.

Woolley, T. E., Gaffney, E. A. & Goriely, A. (2017), 'Random blebbing motion: a simple model linking cell structural properties to migration characteristics', *Phys Rev E* **96**(1), 012409.

Yamada, K. M., Doyle, A. D. & Lu, J. (2022), 'Cell-3d matrix interactions: recent advances and opportunities', *Trends in Cell Biology* **32**(10), 883–95.

617 Zaidel-Bar, R., Ballestrem, C., Kam, Z. & Geiger, B. (2003), 'Early molecular events in the assembly of matrix
618 adhesions at the leading edge of migrating cells', *Journal of Cell Science* **116**(22), 4605–13.

619 Zhu, J. & Mogilner, A. (2016), 'Comparison of cell migration mechanical strategies in three-dimensional matrices:
620 a computational study', *Interface Focus* **6**, 20160040.